# Training a quantum annealing based restricted Boltzmann machine on cybersecurity data

Vivek Dixit, Raja Selvarajan, Muhammad A. Alam, Travis S. Humble and Sabre Kais

Abstract—We present a real-world application that uses a quantum computer. Specifically, we trained a Restricted Boltzmann Machine (RBM) using quantum annealing (QA) to develop an intrusion detection system. RBMs were trained on the ISCX data, which is a benchmark dataset for cybersecurity. For comparison, RBMs were also trained using contrastive divergence (CD) which is a classical method. D-Wave's 2000Q quantum annealer has been used to implement QA. Our analysis of the ISCX data shows that the dataset is imbalanced and we present two different schemes to balance the training dataset before feeding it to a classifier. The first scheme is based on the oversampling of attack instances. The imbalanced training dataset was divided into five sub-datasets that were trained separately. A majority voting was performed to get the final result. Our results show the majority vote increased the classification accuracy up from 90.24% to 95.68% in the case of CD. For the case of QA, the classification accuracy increased from 74.14% to 80.04%. In the second scheme, an RBM was used to generate synthetic data to balance the training dataset. The RBMs trained on synthetic data generated from a CD-trained RBM performed comparably to the RBMs trained on synthetic data generated from a QAtrained RBM. Balanced training data was used to evaluate several classifiers. Among the classifiers investigated, K-Nearest Neighbor (KNN) and Neural Network (NN) performed better than other classifiers. They both showed an accuracy of 93%. Our results show a proof of concept that a QA-based RBM can be trained on a binary dataset, with 64-bit records. The illustrative example suggests the possibility to migrate many practical classification problems to QA-based techniques.

Index Terms—RBM training, D-Wave quantum computer, quantum annealing, machine learning, synthetic data, cybersecurity, ISCX dataset.

#### I. INTRODUCTION

ETWORKS have revolutionized our lives through various purposes including email, file transfer, web search, e-commerce, online banking, monetary transaction, education,

Vivek Dixit, Raja Selvarajan and Sabre Kais are with the Department of Chemistry, Department of Physics and Astronomy, and Purdue Quantum Science and Engineering Institute, Purdue University, West Lafayette, IN, 47907, USA

Muhammad A. Alam is with the Department of Electrical and Computer Engineering, Purdue University, West Lafayette, IN, 47907, USA

Travis S. Humble is with Quantum Computing Institute, Oak Ridge National Laboratory, Oak Ridge, TN, USA

This manuscript has been authored by UT-Battelle, LLC, under Contract No. DE-AC0500OR22725 with the U.S. Department of Energy. The United States Government retains and the publisher, by accepting the article for publication, acknowledges that the United States Government retains a non-exclusive, paid-up, irrevocable, world-wide license to publish or reproduce the published form of this manuscript, or allow others to do so, for the United States Government purposes. The Department of Energy will provide public access to these results of federally sponsored research in accordance with the DOE Public Access Plan.

Manuscript received XXXX; revised XXXX. Corresponding author: Sabre Kais (email: kais@purdue.edu).

collaboration, social networking, etc. The more we depend on it and use it, the more we expose ourselves to serious security risks. The internet represents a vulnerable channel for exchanging information, with a high risk of intrusion and fraud, from phishing, online viruses, trojans, worms, and more. Therefore, there is a need for robust software and devices that protect users from online security threats. An intrusion detection system monitors a network to identify malicious activity or policy violations. Network intrusion detection systems are broadly described by the style of detection employed. Intrusion detection systems rely on misuse-detection by monitoring activity with precise descriptions of known malicious behavior, while anomaly detection systems have a notion of normal activity and flag deviations from that profile [1]. Our work is based on the anomaly detection system, which makes use of machine learning to detect network intrusions by monitoring system activity and classifying it as either benign or attack.

In this work, we have investigated a restricted Boltzmann machine (RBM) based intrusion detection system. An RBM is a generative model, which can model the underlying probability distribution of a dataset. In addition to classifying the class labels, RBMs can also generate a new synthetic dataset. In spite of the importance of the RBMs, only a few investigators have used RBMs for cybersecurity applications. RBM was used by Fiore et al. [2] for intrusion detection, KDD Cup 1999 dataset was used in this study. Aldwairi et al. [3] trained an RBM on the ISCX dataset. This study demonstrated the performance of RBM to classify benign and attack instances, the results show the highest accuracy of 78.7%. Alom et al. [4] studied an intrusion detection system that uses a stack RBM. NSL-KDD dataset was used in this study and the model showed an accuracy of 97.5%. Salama et al. [5] proposed an intrusion detection system where they combined the RBM and support vector machine (SVM). The NSL-KDD dataset was used. The study found that this combination results in higher accuracy than when using SVM only. Alrawashdeh et al. [6] combined the RBM with a deep belief network and used the KDD 1999 data set. The study shows that the RBM classified 92% of the attacks. This paper compared the results to the work by Salama et al. [5] and showed both higher classification accuracy and detection speed.

There are two main problems associated with the use of ML techniques for intrusion detection. The first problem is related to transferability and generalizability of the model, a model trained on a particular dataset performs poorly when tested on other datasets. The second problem is associated with the imbalanced nature of the cybersecurity dataset where the attack instances are outnumbered by benign instances,

which makes detection of an attack like looking for a needle in a haystack. Quantum computing promises to solve these problems. Our work is a step toward that goal. We have used a quantum annealer from D-Wave to train RBMs for intrusion detection applications and compared the performance to RBMs trained with contrastive divergence. Quantum annealers are based on adiabatic quantum annealing (QA), which is a powerful technique for optimization and sampling applications [7], [8], [9], [10]. The D-Wave 2000Q adiabatic quantum computer has been used by several researchers for machine learning applications such as classification, regression, and clustering. Date et al. [11] used a quantum annealer for implementing linear regression. Willsch et al. [12] introduced a method to train support vector machines (SVMs) on a D-Wave 2000Q quantum annealer and compared its performance with classically trained SVMs. Kumar et al. [13] used quantum annealing to carry out the minimization of the clustering objective function. They implemented two clustering algorithms and compared their results with wellknown k-mean clustering. Das et al. [14] used a D-Wave to implement a clustering algorithm for the clustering of charged particle tracks for a hadron collider experiment. Arthur et al. [15] used the D-Wave 2000Q adiabatic quantum computer to train the balanced k-means clustering model. They compared the results with classical k-means and classical balanced kmeans. Kais et al. have used D-Wave's quantum annealer for prime factorization and electronic structure calculation of molecular systems [16], [17]. Adachi et al. [18] trained RBMs using a quantum annealer for a deep belief network (DBN) on a scaled-down MNIST dataset consisting of 32bit binary records. They showed that their model required fewer iterations than CD-based DBN training. Benedetti et al. [19] used quantum annealing to train an RBM on a 16bit binary bars & stripes dataset. Caldeira et al. [20] have used a QA-trained RBM for galaxy morphology classification.

In this work, we trained an RBM using quantum annealing and applied it to the problem of intrusion detection. For comparison purposes, RBMs were also trained with a popular method known as the contrastive divergence. RBMs were trained on the ISCX dataset. ISCX is a cybersecurity dataset that was produced at the Information Security Centre of Excellence at the University of New Brunswick [21]. This is the first use of an RBM trained using QA for intrusion detection. We have also proposed two schemes to balance the ISCX dataset. The first scheme is based on the oversampling of attack records. In the second scheme, synthetic data has been generated from an RBM to balance the training dataset.

Recently, Dixit *et al.* trained an RBM using the D-Wave 2000Q quantum annealer for classification and image reconstruction applications. They used 64-bit bars & stripes dataset in their

### II. METHODS

#### A. Restricted Boltzmann Machine (RBM)

work.

An RBM is an undirected probabilistic graphical model consisting of a layer of hidden variables and a single layer of latent or hidden variables. Each variable is connected to all the variables in the opposite layer, but the connections between the variables in the same layer are not allowed. Let the visible and hidden layers are composed of N and M variables denoted as  $\{v_1, v_2, ..., v_N\}$  and  $\{h_1, h_2, ..., h_M\}$ , respectively. We collectively refer to the visible layer with the vector v and the hidden layer as h. The RBM is an energy-based model with the joint probability distribution specified by its energy function:

$$P(v,h) = \frac{1}{Z}e^{-E(v,h)}, Z = \sum_{v} \sum_{h} e^{-E(v,h)}.$$
 (1)

Z is the normalization constant known as the partition function. The energy function is defined as:

$$E(v,h) = -b^T v - c^T h - h^T W v, \tag{2}$$

2

where b and c are bias vectors at the visible and hidden layer, respectively; W is a weight matrix composed of  $w_{ij}$  elements.

#### B. Conditional Distribution

$$P(h|v) = \frac{P(v,h)}{P(v)} \tag{3}$$

where P(v) is given by the following expression:

$$P(v) = \frac{\sum_{h} e^{-E(v,h)}}{Z}.$$
(4)

Using expression P(v,h) from Eq. 1, we get:

$$P(h|v) = \frac{exp\{\sum_{j} c_j h_j + \sum_{j} (v^T W)_j h_j\}}{Z'}, \qquad (5)$$

where

$$Z' = \sum_{h} exp(c^{T}h + h^{T}Wv). \tag{6}$$

$$P(h|v) = \frac{1}{Z'} \prod_{i} exp\{c_{j}h_{j} + (v^{T}W)_{j}h_{j}\}$$
 (7)

Let's denote

$$\widetilde{P}(h_j|v) = exp\{c_jh_j + (v^TW)_jh_j\}$$
(8)

The probability to find an individual variable in the hidden layer,  $h_i = 1$  is:

$$P(h_{j} = 1|v) = \frac{\widetilde{P}(h_{j} = 1|v)}{\widetilde{P}(h_{j} = 0|v) + \widetilde{P}(h_{j} = 1|v)}$$

$$= \frac{exp\{c_{j} + (v^{T}W)_{j}\}}{1 + exp\{c_{j} + (v^{T}W)_{j}\}}$$
(9)

Thus, the individual hidden activation probability is given by:

$$P(h_j = 1|v) = \sigma\left(c_j + (v^T W)_j\right),\tag{10}$$

where  $\sigma$  is the sigmoid function. Similarly, the activation probability of a visible variable conditioned on a hidden vector h is given by:

$$P(v_i = 1|h) = \sigma(b_i + (h^T W)_i).$$
 (11)

## C. Training RBMs

An RBM is trained by maximizing the likelihood of the training data. The log-likelihood is given by:

$$l(W, b, c) = \sum_{t=1}^{N} \log P(v^{(t)})$$

$$= \sum_{t=1}^{N} \log \sum_{h} P(v^{(t)}, h),$$
(12)

where N is the number of records in the training dataset and  $v^{(t)}$  is a sample from the training dataset.

$$l(W, b, c) = \sum_{t=1}^{N} \log \sum_{h} e^{-E(v^{(t)}, h)}$$
$$-N \cdot \log \sum_{v,h} e^{-E(v, h)}.$$
 (13)

Denote  $\theta = \{W, b, c\}$ . The gradient of the log-likelihood is given by:

$$\nabla_{\theta} l(\theta) = \sum_{t=1}^{N} \frac{\sum_{h} e^{-E(v^{(t)}, h)} \nabla_{\theta} (-E(v^{(t)}, h))}{\sum_{h} e^{-E(v^{(t)}, h)}} - N \cdot \frac{\sum_{v, h} e^{-E(v, h)} \nabla_{\theta} (-E(v, h))}{\sum_{v, h} e^{-E(v, h)}}$$
(14)

$$\nabla_{\theta} l(\theta) = \sum_{t=1}^{N} \langle \nabla_{\theta} (-E(v^{(t)}, h)) \rangle_{P(h|v^{(t)})}$$

$$- N \cdot \langle \nabla_{\theta} (-E(v, h)) \rangle_{P(v, h)},$$
(15)

where  $\langle \cdot \rangle_{P(v,h)}$  is the expectation value with respect to the distribution P(v,h). The gradient with respect to  $\theta$  can also be expressed in terms of its components:

$$\nabla_w l = \frac{1}{N} \sum_{t=1}^N \langle v^{(t)} \cdot h \rangle_{P(h|v^{(t)})} - \langle v \cdot h \rangle_{P(v,h)}$$
 (16)

$$\nabla_b l = \frac{1}{N} \sum_{t=1}^N \langle v^{(t)} \rangle_{P(h|v^{(t)})} - \langle v \rangle_{P(v,h)}$$
 (17)

$$\nabla_c l = \frac{1}{N} \sum_{t=1}^{N} \langle h \rangle_{P(h|v^{(t)})} - \langle h \rangle_{P(v,h)}$$
 (18)

The first term in Eq. 15 is a data-dependent term. It can be exactly calculated using a training vector  $v^{(t)}$  and a hidden vector h. Given  $v^{(t)}$ , the vector h can be calculated using Eq. 10. The second term is a model-dependent term. Getting samples for the second term is difficult. The Contrastive Divergence (CD) is the most commonly used algorithm to determine the model-dependent term. In CD, a training vector is applied to the visible layer. Then the binary states of the hidden units are computed in parallel using Eq. 10. The states of the units on the visible layer are reconstructed using h via Eq. 11. Finally, the reconstructed v is used to find a new h

on the hidden layer. During the RBM training, the change in model parameters is given as:

$$\theta_j^{new} = \theta_j^{old} + \epsilon \cdot \nabla_{\theta_j} l(\theta_j) \tag{19}$$

3

where  $\epsilon$  is the learning rate.

The learning works well even though CD only crudely approximating the gradient of the log probability of the training data. Sutskever et al. [22] have shown that the contrastive divergence does not estimate the gradient of the log-likelihood. An effective method for RBM training is still not known. It has been shown by several researchers that an RBM can be trained using samples drawn from the D-Wave quantum annealer [18] [19] [20] [23]. The first term of the gradient of the log-likelihood is estimated using the procedure explained earlier. The second term which is the model-dependent term is calculated in a different manner. First, an RBM is embedded on to a quantum annealer, then quantum annealing is performed. The samples obtained from quantum annealing is used to compute the second term. The samples from a quantum annealer operating at a temperature T is qualitatively similar to a probability distribution given by  $\exp(\frac{-E(v,h)}{kT})$ . However, to compute the model-dependent term we need samples from a distribution  $e^{-E(v,h)}$  (Eq. 15). To address this problem we scale the energy by a hyperparameter S, such that for the model-dependent term, we sample from  $e^{\frac{-E(v,h)}{SkT}}$  distribution. Here, S is a hyperparameter, which is determined by a manual search. The optimal condition corresponds to the case when SkT = 1. It should be noted as the RBM training starts with random weights and biases and samples from the D-Wave are not expected to show a Boltzmann distribution, however, as the training progresses the underlying probability distribution moves toward the Boltzmann distribution. RBM training using CD-1 and QA is summarized in Algorithm 1 and Algorithm 2, respectively. The two methods differ only in the manner the model-dependent term is estimated.

#### D. The D-Wave Quantum Annealer

To formulate a problem for the D-Wave, one needs to transform the problem into Ising form given by:

$$E(s|h,J) = \sum_{i=1}^{N} h_i s_i + \sum_{i < j}^{N} J_{ij} s_i s_j; \ s_i \in \{-1, +1\}$$
 (20)

This is an objective function of N variables  $s = [s_1, s_2, ..., s_N]$  corresponding to physical Ising spins, where  $h_i$  are the biases and  $J_{ij}$  the couplings between spins.

The energy of an RBM model given by Eq. 2, has a form similar to Eq. 20. The weights and biases of an RBM which is trained using a binary dataset,  $\{0,1\}$  states can be converted to use  $\{-1,1\}$  states via the mapping [24]:

$$b_i' = \frac{b_i}{2} + \frac{\sum_j W_{ij}}{4} \tag{21}$$

$$c_i' = \frac{c_i}{2} + \frac{\sum_j W_{ij}}{4} \tag{22}$$

These weights and biases can be used to embed an RBM onto the D-Wave machine. After executing quantum annealing, solutions can be sampled. We set anneal time to  $20\mu s$  for each anneal. The resulting bipolar samples may be converted to a binary sample simply by replacing all instances of -1 with 0.

The D-Wave adiabatic quantum annealer has 2048 qubits arranged in  $16 \times 16$  unit cells forming a C16 Chimera graph. Each unit cell is composed of 8 qubits connected in a bipartite graph. Each qubit is connected to four other qubits of the same unit cell and two qubits of two different unit cells. One can embed a fully connected RBM of 64 visible and 64 hidden units on a C16 Chimera graph as shown in Fig. 1. In this embedding, each RBM unit is represented by a chain of 16 physical qubits. If we look at the arrangement of qubits, we notice that 16 qubits can be combined by forming a vertical chain. Each vertical chain forms one visible unit. Similarly, 16 horizontal qubits can be linked together to form a hidden unit. In Fig. 1, the vertical chains are shown in red, while the horizontal chains are in black. There are 64 vertical and 64 horizontal chains which represent 64 visible units and 64 hidden units of the RBM. If some qubits in the D-Wave QPU are missing or not working, then the length of the qubit chain forming an RBM unit will be shorter. In that case, the RBM will be not fully connected, that is some connections between visible and hidden units will be missing. Fortunately, in the D-Wave OPU only a very few qubits are missing which does seem to affect the performance of the RBMs. This embedding has also been used in our previous work [23]. A similar bipartite embedding been demonstrated by Goodrich et al. [25].

## Algorithm 1 Optimization of learning parameter using CD-1

- 1:  $\epsilon \leftarrow learning \ rate \quad \triangleright \epsilon$ , is the step size, a small positive number.
- 2:  $b, c, W \leftarrow random \ number$ ▶ Initialize with small normally distributed random numbers.
- 3: while not converged do
- Sample a minibatch of m examples  $\{x^{(1)},...,x^{(m)}\}$  from the training set
- $V \leftarrow \{x^{(1)}, ..., x^{(m)}\}$
- $H \leftarrow \sigma(c + VW)$  $\triangleright \sigma$  is the sigmoid function
- $V' \leftarrow \sigma(b + HW^T)$
- $H' \leftarrow \sigma(c + V'W)$
- $W \leftarrow W + \epsilon \frac{\left(VH V'H'\right)}{m}$   $b \leftarrow b + \epsilon \frac{\left(sum(V) sum(V')\right)}{m}$   $c \leftarrow c + \epsilon \frac{\left(sum(H) sum(H')\right)}{m}$  $\triangleright$  updates W
- $\triangleright$  updates b
- $\triangleright$  updates c

12: end

#### III. RESULTS AND DISCUSSION

#### A. Rationale for preprocessing the imbalanced dataset

The ISCX dataset has been used to perform experiments and evaluate the performance of proposed models. This dataset

Algorithm 2 Optimization of learning parameter using quantum annealing

- 1:  $\epsilon \leftarrow learning \ rate \quad \triangleright \epsilon$ , is the step size, a small positive number.
- 2:  $b, c, W \leftarrow random\ number$ ▶ Initialize with small normally distributed random numbers.
- 3: while not converged do
- Sample a minibatch of m examples  $\{x^{(1)},...,x^{(m)}\}$  from the training set
- $V \leftarrow \{x^{(1)}, ..., x^{(m)}\}$
- $H \leftarrow \sigma(c + VW)$  $\triangleright \sigma$  is the sigmoid function
- $\{h,J\} \leftarrow \{b,c,W\}$
- find hyperparameter S
- $(V', H') \leftarrow quantum \ annealing(h, J, S)$

10: 
$$W \leftarrow W + \epsilon \frac{(VH - V'H')}{m}$$
 > updates W

10: 
$$W \leftarrow W + \epsilon \frac{\left(VH - V'H'\right)}{m}$$
 > updates  $W$ 
11:  $b \leftarrow b + \epsilon \frac{\left(sum(V) - sum(V')\right)}{m}$  > updates  $b$ 
12:  $c \leftarrow c + \epsilon \frac{\left(sum(H) - sum(H')\right)}{m}$  > updates  $c$ 

12: 
$$c \leftarrow c + \epsilon \frac{(sum(H) - sum(H))}{m}$$
  $\Rightarrow$  updates  $c$ 

13: end

has been produced at the Information Security Centre of Excellence at the University of New Brunswick. This dataset has been generated over a period of seven days. It contains normal and attack traffic data. Four different attack types, referred to as Brute Force SSH, Infiltrating, HTTP DoS, and DDoS are conducted and logged along with normal traffic on 7 successive days. In order to investigate the ISCX dataset with an RBM, it is important to preprocess the data and convert the features into a binary form that can be used as a suitable input for the RBM during the different stages of training and testing. Categorical variables were converted to numerical variables. Principle component analysis was then performed to reduce the dimensionality of the dataset. We extracted 16 PCA components for further analysis. Finally, the dataset was binarized by using a supervised discretization filter implemented in Weka [26].

As we discussed in the earlier section one can embed an RBM onto the D-Wave 2000Q with 64 visible and 64 hidden units. Therefore, we set the total number of columns in the binarized dataset to be 64. There were 62 binary features in the dataset and the last two columns were the target variables. When the last two bits were 01, it indicated a benign instance; while 10 indicated an attack. If the last two bits were either a 00 or 11, it indicated an indeterminate case. Thus, the possibility that a random guess could be correct is 25%, and keeping two bits for the target variable helps to prepare a more robust machine learning model as compared to the case where one bit is used as a target variable. The dataset that was obtained after binarization of the original dataset had 137584 instances, however, it was found that most of the records were repeated. The dataset was further modified, and only unique records were retained. There were 25230 unique benign and 4917 unique attack records. Training and test datasets were formed with these records. The test dataset was composed of 500 attack and 500 benign records. The remaining 29147 unique records were used in the training dataset. We trained

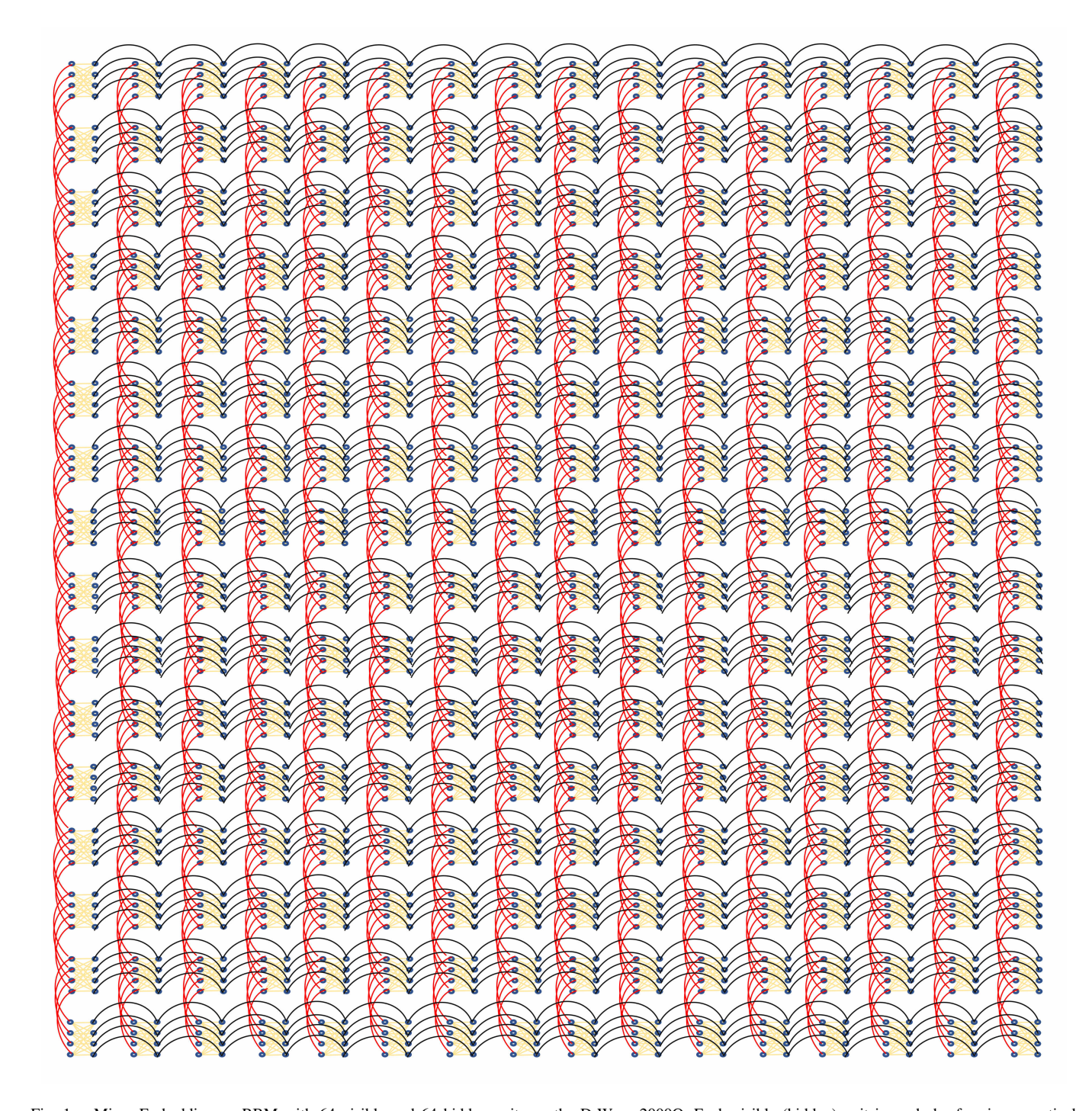


Fig. 1. Minor-Embedding an RBM with 64 visible and 64 hidden units on the D-Wave 2000Q. Each visible (hidden) unit is made by forming a vertical (horizontal) chain of 16 physical qubits shown in red (black).

an RBM on the training dataset. The classification accuracy for the attack class was found to be 42%, while for the benign was 97%. These accuracies were estimated on the test dataset. The lower accuracy for the attack class could be attributed to the fact that there was a significantly higher number of benign instances in the dataset compared to the number of attack instances. The attack records constituted only 14.1% of the total dataset, however, ideally, there should be 50% records of each class. The problem of an imbalanced dataset is commonly seen in cybersecurity datasets; attack records

form a rarer class. Machine learning algorithms show the best results when the number of observations in each class is almost similar. Thus, an imbalanced dataset leads to a poor classification performance of the model. This imbalanced dataset was also investigated using other classification methods, and the results are presented in Table III. To tackle the problem of an imbalanced dataset we propose two schemes. In the first scheme, we used oversampling of the attack class, while in the second scheme an RBM was used to generate instances in order to balance the training dataset. These schemes are

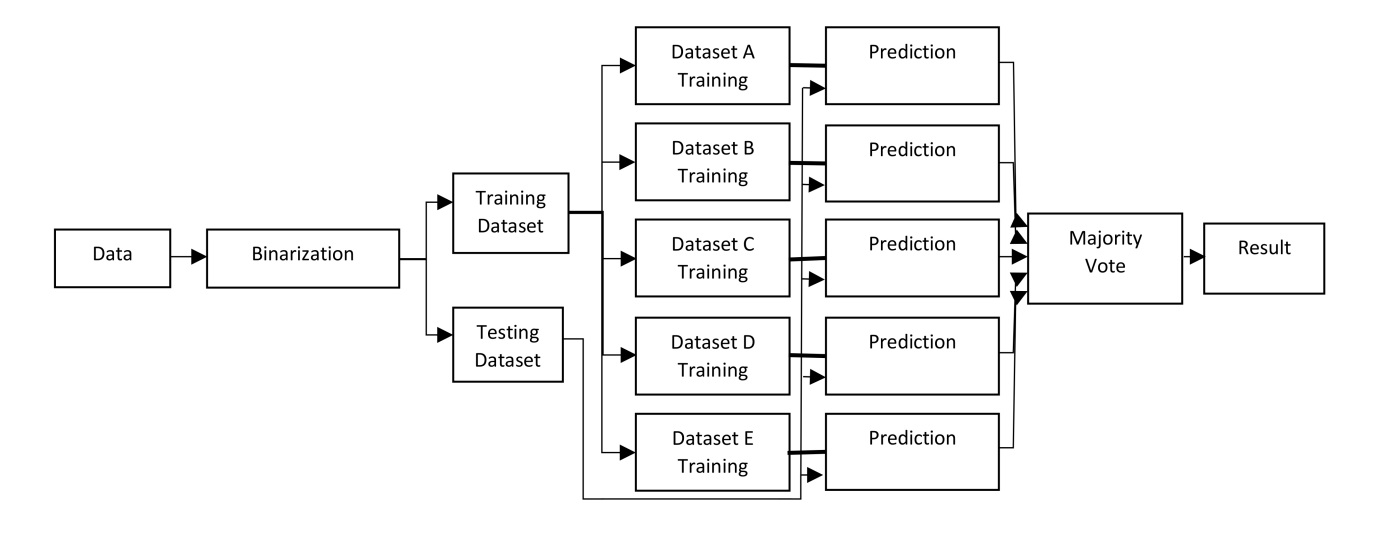


Fig. 2. Scheme 1: Flowchart for intrusion detection using an imbalanced dataset. The training dataset was divided into five balanced datasets which were subsequently used to train five classifiers. The final classification result was obtained by a majority voting.

discussed in more detail in the following sections.

# B. Scheme 1: Balancing training data by oversampling of attack records

Scheme 1 is illustrated in Fig. 2. In this approach, the binarized dataset is divided into training and testing datasets. The training dataset was composed of 21450 records (Benign=18000, Attack=3450), while the test data contained 8697 records (Benign=7230, Attack=1467). Thus, the original binarized dataset was divided into training and testing datasets in the ratio of  $\approx 70\%$ : 30%. The training dataset is further divided into five smaller datasets viz. A, B, C, D, and E. The total number of benign records in the training dataset was divided into five datasets as 18000 = 3450 + 3450 +3450+3450+4200. Thus, each sub-dataset had unique benign records. There were 3450 attack records in the training dataset, we added the same 3450 attack records to each sub-datasets. Sub-dataset E had 4200 (=3450+750) attack records, 750 of which were repeated. Thus, each sub-dataset contained an equal number of instances of both classes. Five RBM models were trained on these five datasets. These trained RBMs models were used to make predictions on the testing dataset. Predictions from the five RBM models were collected and a majority voting was performed to obtain a final result. Two different methods, contrastive divergence (CD-1) and quantum annealing (QA), were employed to train the RBMs. To quantify the performances of the RBMs, the classification accuracy was calculated. Total classification accuracy,  $A_{tot}$ , is defined as:

$$A_{tot} = \frac{n}{N} \times 100, \tag{24}$$

where n is number of correct prediction and N is total number of predictions. While classification accuracy of a class,  $A_c$ , is defined as:

$$A_c = \frac{n_c}{N_c} \times 100, \tag{25}$$

where  $n_c$  is number of correct prediction of a class c and  $N_c$  is total number of predictions of the class c. The results for each case is presented in Table I.

Let us first focus on the results obtained from CD-1 trained RBMs (Table I). The average classification accuracy of the benign class was 90.51% and that of the attack class was 88.94%. The total accuracy was 90.24%. On using the majority vote on the results obtained from five different RBMs, the classification accuracy with which the benign and attack classes can be predicted, and total accuracy was found to be 96.17%, 93.25%, and 95.68%, respectively. In the case where RBMs were trained with quantum annealing, the average classification accuracy of the benign and attack classes, and total accuracy were 73.62% and 71.18%, and 74.14%, respectively. On applying the majority vote on the results from five trained RBMs, the average classification accuracy for the benign, attack classes, and total accuracy were 74.46%, 85.62%, and 80.04%, respectively. Thus, in the case of CD-1 as well as QA, we notice an improvement in accuracy when the majority vote was applied. The strategy to divide the original training dataset into five smaller datasets followed by training five RBMs and then taking the majority vote to get the results seems to be working for the ISCX dataset. Table I also compares the performances of RBMs trained using CD-1 and QA methods. Using the majority vote the total accuracy with CD-1 and OA methods were found to be 95.68% and 80.04%, respectively. Let us consider the results from the individual models, for example, the RBM model trained on sub-dataset A. Dataset A is comprised of just 3450 attack and 3450 benign records, but the classification accuracy of the RBM is better than the case when the training dataset was imbalanced.

The contrastive divergence being a state-of-the-art method for RBM training, a better performance of a CD trained RBM was expected. While CD-1 is a popular and effective method for RBM training, QA for RBM training has not been explored much. Considering the prevailing noise and error-prone nature of the existing quantum machine a classification accuracy of

TABLE I

THE ORIGINAL TRAINING DATASET WAS DIVIDED INTO FIVE SMALL DATASETS (A, B, C, D, AND E). THESE DATASETS WERE USED TO TRAIN FIVE RBMS USING CONTRASTIVE DIVERGENCE (CD-1) AND QUANTUM ANNEALING (QA). CLASSIFICATION ACCURACIES FOR BENIGN AND ATTACK CLASSES, AS WELL AS TOTAL ACCURACY, ARE PRESENTED FOR EACH DATASET. VALUES ARE EVALUATED ON THE TESTING DATA. A MAJORITY VOTE WAS ALSO PERFORMED ON THE RESULTS OBTAINED FROM FIVE RBMS.

Dataset	No. of records	Accuracy, A <sub>benign</sub>		Accuracy,	$A_{attack}$	Total Accuracy, A <sub>tot</sub>	
Buttaset	110. of feeding	CD-1 (%)	QA (%)	CD-1 (%)	QA (%)	CD-1 (%)	QA (%)
A	6900	92.17	82.60	88.75	68.30	91.59	80.19
В	6900	88.30	71.76	88.82	72.60	88.39	71.90
C	6900	90.11	69.04	89.23	83.01	89.96	76.03
D	6900	90.03	67.65	90.52	72.73	90.11	68.51
E	8400	91.94	77.05	87.39	59.24	91.17	74.05
Average	_	90.51	73.62	88.94	71.18	90.24	74.14
Standard deviation	_	1.59	6.17	1.12	8.59	1.25	4.38
Majority Vote	_	96.17	74.46	93.25	85.62	95.68	80.04

80.04% seems to be satisfactory. Our goal here is to show a proof of concept that RBM can be trained using quantum annealing on a 64-bit binary dataset. RBM training using QA can be improved by optimizing D-Wave annealing parameters like anneal time, chain length, etc. Further, an efficient way to calculate the quantum annealer's effective temperature can also improve QA-based RBM training.

# C. Scheme 2: Balancing training dataset by using synthetic data

A dataset is said to be imbalanced if the number of observations in each class is not proportionate. Generally, when we deal with a cybersecurity dataset, we face the problem of a lower number of attack instances compare to the benign instances. Previously, we showed this problem could be solved by creating several small sub-datasets and subsequently using those to train individual models, and finally reaching a result by performing a majority vote. Another way to deal with this problem is to generate synthetic data using an RBM and then using the synthetic data to balance the training dataset.

In this section, we will discuss how we used synthetic data generated from a trained RBM to balance the training dataset. A synthetic data sample can be generated from an RBM trained using CD-1 in the following way. We input a 64-bit vector formed using random 0s and 1s to a trained RBM. After 50 Gibbs cycles, we sample a 64-bit binary vector from the visible layer of the RBM. This sampled binary vector forms an instance of the synthetic dataset. Generating a synthetic dataset using QA is straightforward. The first step is to embed a trained RBM onto the D-Wave, then we perform quantum annealing and request 10000 samples. For quantum annealing the anneal time was set to  $20\mu s$  for each anneal. From each sample, the states of the visible units are determined. Each sample corresponds to a record in the synthetic dataset. In this way, synthetic data composed of 10000 records is obtained using QA.

To ensure that the synthetic dataset generated from a trained RBM is useful, we performed the following experiment. We used trained RBM models (A, B, C, D, and E) from the previous experiment to generate synthetic datasets; one from each model. Thus, ten datasets were generated; five from CD-based RBMs and the other five from QA-based RBMs.

Now, ten RBM models were trained on these ten synthetic datasets using CD-1. The performance of these ten RBM models was compared by estimating classification accuracies on the test dataset composed of 8697 records (Benign=7230, Attack=1467). The results from these RBM models as well as estimated average and standard deviation are presented in Table II. RBMs trained using synthetic dataset generated from 'CD-1 trained RBM' showed total classification accuracy varying between 64.63% to 79.31%. While RBM trained with synthetic dataset obtained from 'QA trained RBM' showed classification accuracy varying between 64.32% to 79.42%. Average classification accuracy for benign and attack classes were 68.28% and 85.66% with dataset obtained from CD-1 based RBM, and 67.47% and 72.90% with dataset obtained from QA based RBM. The results from Table II indicate that useful synthetic data can be generated from a trained RBM. This synthetic data can be used to augment the original imbalanced training dataset in order to balance it. Also, on the basis of the classification accuracies, one can conclude that the samples obtained from an RBM trained using QA are as good as from an RBM trained with CD-1.

Now we know that an RBM can be used to generate useful synthetic data. We can use this procedure to generate synthetic data to balance the training data and hence improve the performance of a classifier. Scheme 2, which uses an RBM to generate new data, is illustrated in Fig. 3. The original dataset is first binarized and divided into testing and training data. The training data is used to train an RBM, which is subsequently used to generate a synthetic dataset. Depending on the number of instances needed to balance the training data, one can use a subset of a synthetic dataset to balance the training dataset. There were 18000 benign and 3450 attack records in the training dataset, so 14550 synthetic attack records were added to balance the training dataset. A classifier is then trained on the balanced dataset and a prediction on the original testing data is performed.

Considering the fact that RBMs are mostly used as a generative model and there are other classification methods that may perform better than an RBM classifier, we trained several classifiers on the balanced training dataset. The results are presented in Table III. For comparison, model performance with the original imbalanced dataset is also included. To compare and quantify the performances of different methods,

#### TABLE II

SYNTHETIC DATASETS WERE GENERATED FROM RBMS TRAINED USING CONTRASTIVE DIVERGENCE (CD) AND QUANTUM ANNEALING (QA). THESE SYNTHETIC DATASETS WERE THEN USED TO TRAIN RBMS USING CD. THE CLASSIFICATION ACCURACIES OF THESE RBMS FOR BENIGN AND ATTACK RECORDS, AS WELL AS TOTAL ACCURACIES, ARE PRESENTED. THESE ACCURACIES ARE CALCULATED ON THE TESTING DATASET. THE LABEL 'MODEL' INDICATES THE RBM MODEL THAT WAS USED TO GENERATE THE SYNTHETIC DATASET.

Model	Classification Accuracy			Model	Classification Accuracy			
	Benign (%)	Attack (%)	Total (%)	Wiodei	Benign (%)	Attack (%)	Total (%)	
A-CD	78.99	80.91	79.31	A-QA	63.35	76.89	65.63	
B-CD	73.26	84.32	75.13	B-QA	67.34	73.62	68.40	
C-CD	59.35	90.66	64.63	C-QA	72.28	66.73	79.42	
D-CD	61.69	87.12	65.98	D-QA	72.89	69.05	72.24	
E-CD	68.13	85.28	71.02	E-QA	61.51	78.19	64.32	
Average	68.28	85.66	71.21	Average	67.47	72.90	70.00	
Stdev	8.10	3.59	6.16	Stdev	5.12	4.93	6.08	

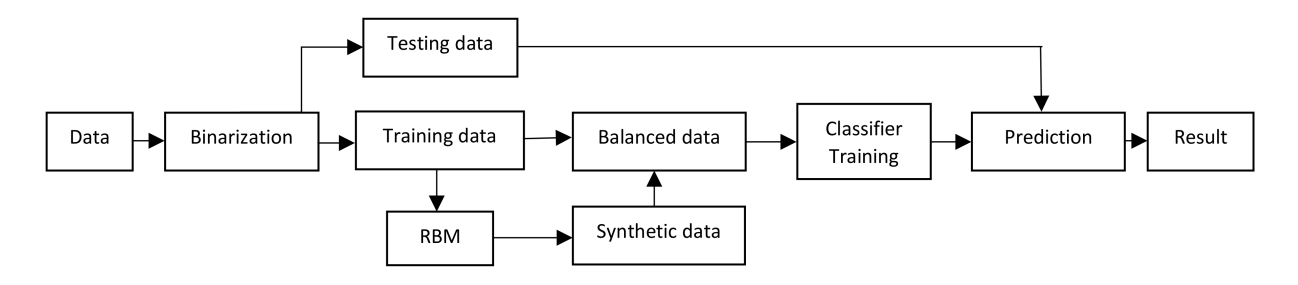


Fig. 3. Scheme 2: Flowchart for intrusion detection using an imbalanced dataset. An RBM was first trained using the training dataset and then it was used to generate synthetic data. Training data and synthetic data were used to create a balanced dataset which was further used to train a classifier.

#### TABLE III

Balanced training data was used to train six classifiers. Performance metrics: precision, recall,  $F_1$  score, and accuracy were used to compare models. The label 'CD-bal' ('QA-bal') indicates that the synthetic data that was used to balance the training dataset was obtained from an RBM trained with contrastive divergence (quantum annealing). The label 'imbal' indicates the original imbalanced dataset. Values are evaluated on the testing data.

Method	Data	Precision Attack Benign		Recall Attack Benign		F <sub>1</sub> score Attack Benign		Accuracy, A <sub>tot</sub>	
Restricted	CD-bal	0.87	0.94	0.95	0.85	0.91	0.89	85%	
Boltzmann	OA-bal	0.92	0.82	0.80	0.93	0.85	0.87	82%	
Machine	imbal	0.93	0.63	0.42	0.97	0.58	0.77	68%	
Neural	CD-bal	0.95	0.90	0.89	0.96	0.92	0.93	93%	
Network	QA-bal	0.95	0.90	0.89	0.96	0.92	0.93	93%	
(NN)	imbal	1.00	0.60	0.32	1.00	0.49	0.75	66%	
K-Nearest	CD-bal	0.98	0.89	0.87	0.98	0.92	0.93	93%	
Neighbor	QA-bal	0.98	0.89	0.87	0.98	0.92	0.93	93%	
(KNN)	imbal	1.00	0.62	0.40	1.00	0.57	0.77	70%	
Support	CD-bal	0.94	0.77	0.70	0.95	0.80	0.86	83%	
Vector	QA-bal	0.94	0.77	0.70	0.95	0.80	0.85	83%	
Classifier	imbal	1.00	0.58	0.26	1.00	0.42	0.73	63%	
	CD-bal	0.90	0.83	0.80	0.92	0.85	0.87	86%	
Decision Tree	QA-bal	0.90	0.83	0.80	0.92	0.85	0.87	86%	
	imbal	1.00	0.56	0.22	1.00	0.36	0.72	61%	
Naive Bayes	CD-bal	0.87	0.60	0.33	0.95	0.48	0.74	65%	
	QA-bal	0.87	0.60	0.33	0.95	0.48	0.74	65%	
	imbal	1.00	0.54	0.16	1.00	0.27	0.70	58%	

matrics based on confusion matrix are used. A confusion matrix is a table that is used to describe the performance of a classifier on a test dataset for which true values are known. Basic terms used in a confusion matrix are the following:

- True positive (TP): Observation is positive, and is predicted to be positive.
- False negative (FN): Observation is positive, but is predicted negative.
- True negative (TN): Observation is negative, and is predicted to be negative.
- False positive (FP): Observation is negative, but is predicted positive.

Following measures were used to compare the performance of the classifiers:

$$Precision = \frac{TP}{TP + FP} \tag{26}$$

$$Recall = \frac{TP}{TP + FN} \tag{27}$$

$$Recall = \frac{TP}{TP + FN}$$

$$F_1score = 2 \times \frac{Precision \times Recall}{Precision + Recall}$$
(28)

From Table III, we notice that K Nearest Neighbor (KNN) and Neural Network (NN) performed better than other models. They both showed a classification accuracy of 93%. Their values for precision, recall, and  $F_1$  scores were also better than other methods. The lowest value of classification accuracy, as well as other metrics, was found in the case of Naive Bayes. The classification accuracy for this classifier was 65%. This exercise shows that it is important to investigate different classifiers to achieve better performance and different methods may give widely differing results. Table III shows that each classification method showed improved performance when the dataset was balanced. Thus, the technique used to balance the dataset using synthetic data was effective. This demonstrates the ability of the RBM to fill gaps in an imbalanced dataset by creating synthetic data that falls within the probability range of existing data.

#### IV. CONCLUSIONS

An RBM-based intrusion detection system has been developed using the cybersecurity ISCX dataset. RBMs were trained using samples obtained from the D-Wave 2000O quantum annealer. For comparison, a state-of-the-art method for RBM training, contrastive divergence, was also investigated. The ISCX dataset was preprocessed and binarized to transform it into a form that can be used with an RBM. When a classifier was trained on the original data, it was found that attack records can be correctly predicted with an accuracy of 42%, while benign records with an accuracy of 97%. This disproportionate result was attributed to the fact that the dataset was imbalanced. The attack records in the dataset only accounted for 14.1% of the total number of records. To deal with the imbalanced dataset, we came up with two schemes. The first scheme was based on the oversampling of attack records. In this scheme, the training dataset was divided into five sub-datasets. Five classifiers were trained separately on these datasets. The final result was obtained by performing a majority voting on the results from the individual classifiers. Our results show that by using a majority vote the classification accuracy increased up to 95.68% from 90.24% in the case of CD-1. While in the case of OA, the classification accuracy increased to 80.04% from 74.14%. The second scheme that we used to balance the training dataset was based on the generation of synthetic data using a trained RBM. The results indicate that for the sampling application an RBM trained with QA is as good as an RBM trained with CD. The balanced dataset obtained from this scheme was used to train six different classifiers. Neural network and K-nearest neighbor models performed better than other classifiers. Based on classification accuracy results, we infer that both scheme 1 and scheme 2 performed comparably. The learning of QAbased RBM can be improved with the availability of improved quantum annealers with a higher number of qubits as well as by using the actual effective temperature of the QPU instead of a hyperparameter S.

#### ACKNOWLEDGMENT

We are grateful for the support from Integrated Data Science Initiative Grants (IDSI F.90000303), Purdue University. S.K. would like to acknowledge funding by the U.S. Department of Energy (Office of Basic Energy Sciences) under Award No. DE-SC0019215. T.S.H. would like to acknowledge funding by the U.S. Department of Energy, Office of Basic Energy Science. This research used resources of the Oak Ridge Leadership Computing Facility, which is a DOE Office of Science User Facility supported under Contract DE-AC05-00OR22725. V.D. would like to thank Y. Koshka and M.A. Novotny for useful discussions on restricted Boltmann machines.

#### REFERENCES

- [1] C. Ko, M. Ruschitzka, and K. Levitt, "Execution monitoring of securitycritical programs in distributed systems: A specification-based approach," in Proceedings. 1997 IEEE Symposium on Security and Privacy (Cat. No. 97CB36097). IEEE, 1997, pp. 175-187.
- [2] U. Fiore, F. Palmieri, A. Castiglione, and A. De Santis, "Network anomaly detection with the restricted boltzmann machine," Neurocomputing, vol. 122, pp. 13-23, 2013.
- [3] T. Aldwairi, D. Perera, and M. A. Novotny, "An evaluation of the performance of restricted boltzmann machines as a model for anomaly network intrusion detection," Computer Networks, vol. 144, pp. 111-119, 2018.
- [4] M. Z. Alom, V. Bontupalli, and T. M. Taha, "Intrusion detection using deep belief networks," in 2015 National Aerospace and Electronics Conference (NAECON). IEEE, 2015, pp. 339-344.
- [5] M. A. Salama, H. F. Eid, R. A. Ramadan, A. Darwish, and A. E. Hassanien, "Hybrid intelligent intrusion detection scheme," in Soft computing in industrial applications. Springer, 2011, pp. 293-303.
- [6] K. Alrawashdeh and C. Purdy, "Toward an online anomaly intrusion detection system based on deep learning," in 2016 15th IEEE international conference on machine learning and applications (ICMLA). IEEE, 2016, pp. 195-200.
- [7] E. Farhi, J. Goldstone, S. Gutmann, and M. Sipser, "Quantum computation by adiabatic evolution," arXiv preprint quant-ph/0001106, 2000.
- [8] D. Aharonov, W. van Dam, J. Kempe, Z. Landau, S. Lloyd, and O. Regev, "Adiabatic quantum computation is equivalent to standard quantum computation," SIAM Journal on Computing, vol. 37, no. 1, pp. 166-194, 2007. [Online]. Available: https: //doi.org/10.1137/S0097539705447323
- [9] T. Kadowaki and H. Nishimori, "Quantum annealing in the transverse ising model," Phys. Rev. E, vol. 58, pp. 5355-5363, Nov 1998. [Online]. Available: https://link.aps.org/doi/10.1103/PhysRevE.58.5355
- [10] A. Finnila, M. Gomez, C. Sebenik, C. Stenson, and J. Doll, "Quantum annealing: A new method for minimizing multidimensional functions," Chemical Physics Letters, vol. 219, no. 5, pp. 343 - 348, 1994. [Online]. Available: http://www.sciencedirect.com/science/article/ pii/0009261494001170
- [11] T. Potok et al., "Adiabatic quantum linear regression," arXiv preprint arXiv:2008.02355, 2020.
- [12] D. Willsch, M. Willsch, H. De Raedt, and K. Michielsen, "Support vector machines on the d-wave quantum annealer," Computer Physics Communications, vol. 248, p. 107006, 2020. [Online]. Available: http://www.sciencedirect.com/science/article/pii/S001046551930342X
- [13] V. Kumar, G. Bass, C. Tomlin, and J. Dulny, "Quantum annealing for combinatorial clustering," Quantum Information Processing, vol. 17, no. 2, p. 39, 2018.
- S. Das, A. J. Wildridge, S. B. Vaidya, and A. Jung, "Track clustering with a quantum annealer for primary vertex reconstruction at hadron colliders," arXiv preprint arXiv:1903.08879, 2019.
- [15] D. Arthur et al., "Balanced k-means clustering on an adiabatic quantum computer," arXiv preprint arXiv:2008.04419, 2020.
- [16] S. Jiang, K. A. Britt, A. J. McCaskey, T. S. Humble, and S. Kais, "Quantum annealing for prime factorization," Nature Scientific reports,
- R. Xia, T. Bian, and S. Kais, "Electronic structure calculations [17] and the ising hamiltonian," The Journal of Physical Chemistry B, vol. 122, no. 13, pp. 3384-3395, 2018. [Online]. Available: https://doi.org/10.1021/acs.jpcb.7b10371

- [18] S. H. Adachi and M. P. Henderson, "Application of quantum annealing to training of deep neural networks," arXiv preprint arXiv:1510.06356, 2015.
- [19] M. Benedetti, J. Realpe-Gómez, R. Biswas, and A. Perdomo-Ortiz, "Estimation of effective temperatures in quantum annealers for sampling applications: A case study with possible applications in deep learning," *Phys. Rev. A*, vol. 94, p. 022308, Aug 2016. [Online]. Available: https://link.aps.org/doi/10.1103/PhysRevA.94.022308
- [20] J. Caldeira, J. Job, S. H. Adachi, B. Nord, and G. N. Perdue, "Restricted boltzmann machines for galaxy morphology classification with a quantum annealer," arXiv preprint arXiv:1911.06259, 2019.
- [21] A. Shiravi, H. Shiravi, M. Tavallaee, and A. A. Ghorbani, "Toward developing a systematic approach to generate benchmark datasets for intrusion detection," *computers & security*, vol. 31, no. 3, pp. 357–374, 2012.
- [22] I. Sutskever and T. Tieleman, "On the convergence properties of contrastive divergence," in *Proceedings of the thirteenth international* conference on artificial intelligence and statistics, 2010, pp. 789–795.
- [23] V. Dixit, R. Selvarajan, M. A. Alam, T. S. Humble, and S. Kais, "Training and classification using a restricted boltzmann machine on the d-wave 2000q," arXiv preprint arXiv:2005.03247, 2020.
- [24] V. Dumoulin, A. C. Ian J Goodfellow, and Y. Bengio, "On the challenges of physical implementations of rbms," AAAI Publications, Twenty-Eighth AAAI Conference on Artificial Intelligence, 2014. [Online]. Available: https://www.aaai.org/ocs/index.php/AAAI/AAAI14/ paper/viewPaper/8608
- [25] T. D. Goodrich, B. D. Sullivan, and T. S. Humble, "Optimizing adiabatic quantum program compilation using a graph-theoretic framework," *Quantum Information Processing*, vol. 17, April 2018. [Online]. Available: https://doi.org/10.1007/s11128-018-1863-4
- [26] I. H. Witten and E. Frank, "Data mining: practical machine learning tools and techniques with java implementations," *Acm Sigmod Record*, vol. 31, no. 1, pp. 76–77, 2002.

**Vivek Dixit** received the M.S. and Ph.D. degrees in physics and applied physics both from Mississippi State University, Starkville, MS, USA in 2011, and 2015, respectively. He is a postdoctoral research associate in the department of chemistry, Purdue University, West Lafayette, IN, USA. His research interests include Quantum Machine Learning, Quantum Computing, electronic structure calculations of solids and molecular systems, and spectroscopy.

**Raja Selvarajan** is a graduate student in the department of physics and astronomy, Purdue University, West Lafayette, IN, USA. His research interests include Quantum Machine Learning and Quantum Computing.

**Muhammad A. Alam** (M96, SM01, F06) is the Jai N. Gupta professor of Electrical Engineering at Purdue University, where his research focuses on physics, simulation, characterization and technology of classical and emerging electronic devices, including reliability of scaled MOSFET, theoretical foundation of nano-bio sensors, and atom-to-farm performance and modeling of solar cells. His work has been recognized by 2006 IEEE Kiyo Tomiyasu Medal, 2015 SRC Technical Excellence Award, and 2018 IEEE EDS Education Award.

Travis S. Humble is Deputy Director at the Department of Energy's Quantum Science Center, a Distinguished Scientist at Oak Ridge National Laboratory, and director of the lab's Quantum Computing Institute. Travis is leading the development of new quantum technologies and infrastructure to impact the DOE mission of scientific discovery through quantum computing. He is editorin-chief for ACM Transactions on Quantum Computing, Associate Editor for Quantum Information Processing, and co-chair of the IEEE Quantum Initiative. Travis also holds a joint faculty appointment with the University of Tennessee Bredesen Center for Interdisciplinary Research and Graduate Education, where he works with students in developing energy-efficient computing solutions. He received his doctorate in theoretical chemistry from the University of Oregon before joining ORNL in 2005.

Sabre Kais received the BSc, MSc, and PhD degrees at the Hebrew University of Jerusalem in 1983, 1984, and 1989 respectively. From 1989 to 1994, he was a research associate at Harvard University, Department of Chemistry. He joined Purdue University in1994 as an assistant professor of theoretical chemistry. Currently, he is a full professor of chemical physics, a professor of computer science (courtesy), a professor of physics at Purdue University. He has published over 240 papers in peer-reviewed journals. His research interests mainly include finite size scaling, dimensional scaling, Quantum Information, and Quantum Computing, He was the director of NSF funded center of innovation on "Quantum Information for Quantum Chemistry", from 2010-2013. He is a Fellow of the American Physical Society, Fellow of the American Association for the Advancement of Science, Guggenheim Fellow, Purdue University Faculty Scholar, National Science Foundation Career Award Fellow He is a recipient of the 2012 Sigma Xi Research Award, and 2019 Herbert Newby McCoy Award, Purdue University.